Oscillatory regimes of the thermomagnetic instability in superconducting films

J. I. Vestgården,[1,2] Y. M. Galperin,[1,3] and T. H. Johansen[1,4]

[1]*Department of Physics, University of Oslo, P. O. Box 1048 Blindern, 0316 Oslo, Norway*

[2]*Norwegian Defence Research Establishment (FFI), Kjeller, Norway*

[3]*Ioffe Physical Technical Institute, 26 Polytekhnicheskaya, St. Petersburg 194021, Russia*

[4]*Institute for Superconducting and Electronic Materials, University of Wollongong, Innovation Campus, Squires Way, North Wollongong NSW 2500, Australia*

The stability of superconducting films with respect to oscillatory precursor modes for thermomagnetic avalanches is investigated theoretically. The results for the onset threshold show that previous treatments of nonoscillatory modes have predicted much higher thresholds. Thus, in film superconductors, oscillatory modes are far more likely to cause thermomagnetic breakdown. This explains the experimental fact that flux avalanches in film superconductors can occur even at very small ramping rates of the applied magnetic field. Closed expressions for the threshold magnetic field and temperature, as well oscillation frequency, are derived for different regimes of the oscillatory thermomagnetic instability.

The irreversible electromagnetic properties of type-II superconductors are commonly explained in terms of the critical current density j_c, as introduced by Bean [1]. In the corresponding critical state, the distribution of magnetic flux is nonuniform and metastable. However, since j_c is a decreasing function of temperature, the metastable state can become unstable driven by the Joule heat generated during flux motion. In bulk superconductors, this thermomagnetic instability gives rise to abrupt displacement of large amounts of flux, so-called flux jumps, which may cause the entire superconductor to be heated to the normal state [2–6]. In some cases, pronounced oscillations in magnetization and temperature have been detected prior to such jumps [7,8].

In film superconductors experiencing an increasing transverse magnetic field, the thermomagnetic instability gives rise to abrupt flux entry in the form of dendritic structures rooted at the sample edge [9]. Using magneto-optical imaging [10], the residual flux distribution left in the film after such avalanche events has been observed in many superconducting materials [11–14]. The experiments also show that there is a threshold magnetic field, H_{th}, for the onset of avalanche activity, and that the unstable behavior is restricted to temperatures below a threshold value, T_{th}; see Fig. 1. These thresholds have been explained on the basis of linear stability analysis of the nonlinear and nonlocal equations governing the electrodynamics of such films [15–20]. The theoretical works show that in order to trigger avalanches, an electrical field in the range $E = 30$–100 mV/m is required.

Experimentally, one finds in films of many materials, e.g., MgB$_2$, Nb, and NbN, that avalanches occur even when the magnetic field is ramped very slowly, e.g., below 1 mT/s [21], inducing correspondingly small E-fields. For a film placed in a magnetic field ramped at a rate of $\mu_0 \dot{H}_a$ the Bean model estimates [22] the E-field along the edge as $E \sim \mu_0 \dot{H}_a w$, where w is the half-width of the film. With a size of a few millimeters and a ramping rate of 1 mT/s, the edge field is $E \sim 1$ μV/m, i.e., several orders of magnitude below the theoretical threshold. Hence, thermomagnetic avalanches should not occur at such ramping rates, quite contrary to experiment.

This inconsistency led to the suggestion [19] that large local E-fields are created by nonthermomagnetic microavalanches, which in turn trigger the large and devastating [23] events. From a modeling viewpoint, this idea poses severe challenges since the proposed microavalanche scenarios [24–27] have not yet allowed evaluation of the E-fields.

In the present work, earlier analyses of the onset conditions for thermomagnetic avalanches are generalized by including modes with complex instability increments. Thus, scenarios involving oscillatory precursor behavior are considered herein. It is found that such modes, depending on the material parameters, can have much lower thresholds compared to those of the nonoscillatory ones. As a result, the thermomagnetic instability can develop directly from the low E-field background of the Bean critical state, without assuming the existence of microavalanches of an unspecified nature.

Consider a superconducting film shaped as a strip of thickness d and width $2w$, where $w \gg d$. The strip is very long in the y direction, and it is in thermal contact with the substrate; see Fig. 2. The sample is initially zero-field-cooled to a temperature, T, below the superconducting transition temperature, T_c, whereupon a perpendicular magnetic field H_a is applied at a constant rate $\dot{H}_a$. The overall flux dynamics in the superconductor is assumed to follow the Bean model. The magnetic flux then penetrates to a depth l, which increases with the field as [28]

$$l/w = 1 - \cosh^{-1}(\pi H_a / d j_c). \tag{1}$$

This flux motion induces an electrical field, which is maximum at the strip edge where the value is given by [22]

$$E_{edge} = \mu_0 \dot{H}_a w \tanh(\pi H_a / d j_c). \tag{2}$$

For perturbations of the Bean state, we describe the superconductor using the more general model [15]

$$\mathbf{E} = \begin{cases} \rho_n (J/d j_c)^{n-1} \mathbf{J}/d, & J < d j_c \text{ and below } T_c, \\ \rho_n \mathbf{J}/d & \text{otherwise.} \end{cases} \tag{3}$$

Here, $\mathbf{J}$ is the sheet current, ρ_n is the normal state resistivity, and n is the flux creep exponent. The Bean model corresponds to the limit $n \to \infty$.
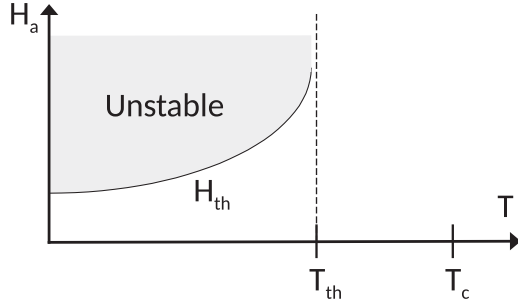
FIG. 1. Generic thermomagnetic stability diagram of film superconductors.

The electrodynamics follows the Maxwell equations:

$$\dot{\mathbf{B}} = -\nabla \times \mathbf{E}, \quad \nabla \times \mathbf{H} = \mathbf{J}\delta(z), \quad \nabla \cdot \mathbf{B} = \mathbf{0}, \quad (4)$$

with $\nabla \cdot \mathbf{J} = 0$, $\mu_0 \mathbf{H} = \mathbf{B}$. The heat flow in the strip is described by

$$c\dot{\tilde{T}} = \kappa \nabla^2 \tilde{T} - \frac{h}{d}(\tilde{T} - T) + \frac{1}{d}\mathbf{J} \cdot \mathbf{E}, \quad (5)$$

where $\tilde{T}$ is the local temperature in the superconductor, and T is the uniform substrate temperature. The superconductor's specific heat is c, its thermal conductivity is κ, and h is the coefficient of heat transfer between the strip and the substrate. The temperature dependencies are chosen as $c = c_0(\tilde{T}/T_c)^3$, $\kappa = \kappa_0(\tilde{T}/T_c)^3$, and $h = h_0(\tilde{T}/T_c)^3$. For the electrodynamical parameters, we use $j_c = j_{c0}(1 - \tilde{T}/T_c)$ and $n = n_0 T_c/\tilde{T}$.

To determine the conditions for the onset of oscillatory regimes of the instability, consider the threshold electric field, E_{th}, following from linearization of Eqs. (3)–(5). As shown in Ref. [29], this gives

$$\frac{j_c}{T^*}nE_{\text{th}} - \kappa k^2 - \frac{h}{d} - \frac{2}{k}\left(k_x^2 + \frac{k_y^2}{n}\right)\frac{c}{\mu_0 d j_c}nE_{\text{th}} = 0, \quad (6)$$

where $T^* = |\partial \ln j_c/\partial T|^{-1}$, and k_x, k_y, and $k = \sqrt{k_x^2 + k_y^2}$ are the Fourier space wave vectors. The instability onset is
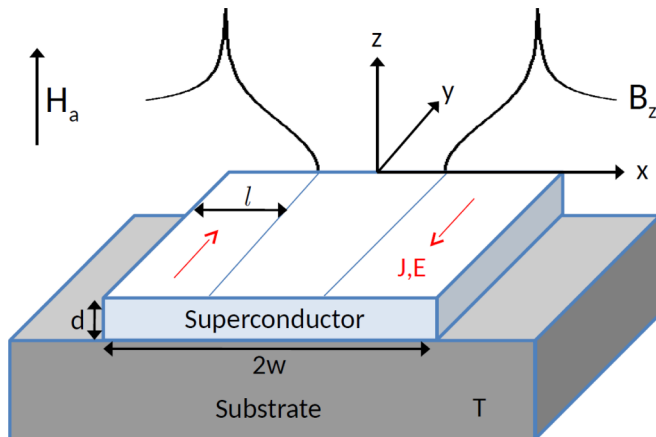
FIG. 2. Sample geometry: A long superconducting strip in thermal contact with a substrate and exposed to an increasing magnetic field H_a applied along the z axis, inducing currents and electrical fields in the y direction.

accompanied by temporal oscillations with frequency

$$\omega^2 = \frac{2}{k}\frac{nE_{\text{th}}}{\mu_0 d j_c c}\left[\left(k_x^2 + \frac{k_y^2}{n}\right)\left(\kappa k^2 + \frac{h}{d}\right) + \left(k_x^2 - k_y^2\right)\frac{j_c E_{\text{th}}}{T^*}\right]. \quad (7)$$

As H_a increases from zero, the most unstable modes correspond to $k_y = 0$ and $k_x = \pi/2l$, and in what follows only these modes are considered.

First, at small H_a, the main mechanism for suppression of the instability is the lateral heat diffusion. Thus, neglecting in Eq. (6) the terms proportional to c and h, one obtains

$$E_{\text{th},\kappa} = \frac{\kappa T^*}{n j_c}\left(\frac{\pi}{2l}\right)^2. \quad (8)$$

For small H_a, Eq. (1) gives $l \approx (w/2)(\pi H_a/d j_c)^2$, and from Eq. (2) the electric field is $E_{\text{edge}} \approx \mu_0 \dot{H}_a w\pi H_a/d j_c$. Inserting these expressions in Eq. (8), the threshold applied magnetic field becomes

$$H_{\text{th},\kappa} = \frac{d j_c}{\pi}\left(\frac{\pi^2 \kappa T^*}{n w^3 j_c \mu_0 \dot{H}_a}\right)^{1/5}. \quad (9)$$

This formula gives the threshold field as a function of temperature through the parameters κ, j_c, and n. The corresponding oscillation frequency, obtained from Eq. (7) assuming $n \gg 1$, is

$$\omega_\kappa = \mu_0 \dot{H}_a n\sqrt{\frac{2\pi w}{\mu_0 d c T^*}}, \quad (10)$$

which depends on temperature through n, c, and T^*.

Then, at deeper penetration, when $l \gg (\pi/2)\sqrt{\kappa d/h}$, the main mechanism suppressing the instability is heat removal by the substrate. In this case, one can ignore in Eq. (6) the terms proportional to κ and c, which gives

$$E_{\text{th},h} = \frac{h T^*}{n d j_c}. \quad (11)$$

Combining this with Eq. (2) to eliminate the E-field, one obtains the following threshold magnetic field:[1]

$$H_{\text{th},h} = \frac{d j_c}{\pi}\,\text{atanh}\left(\frac{h T^*}{n w d j_c \mu_0 \dot{H}_a}\right). \quad (12)$$

Also this case is accompanied by oscillations, and at full penetration, when $E_{\text{edge}} \approx \mu_0 \dot{H}_a w$, the frequency is $\omega_h = \omega_\kappa/\sqrt{2}$. Thus, ω_h and ω_κ are not very different in magnitude, and they have a common temperature dependence.

From Eq. (12) it follows that $H_{\text{th},h}$ diverges when the parameters satisfy the equality

$$h T^*/(n w d j_c \mu_0 \dot{H}_a) = 1.$$

When the left-hand side exceeds unity the instability will not occur, and it is therefore the condition determining the threshold temperature, T_{th}. Thus, one finds

$$T_{\text{th}}/T_c = (n_0 w d j_{c0} \mu_0 \dot{H}_a/T_c h_0)^{1/4}, \quad (13)$$

using the above temperature dependencies of j_c, n, and h.

---

[1] The low-T limit of Eq. (12) was considered also in Ref. [15].
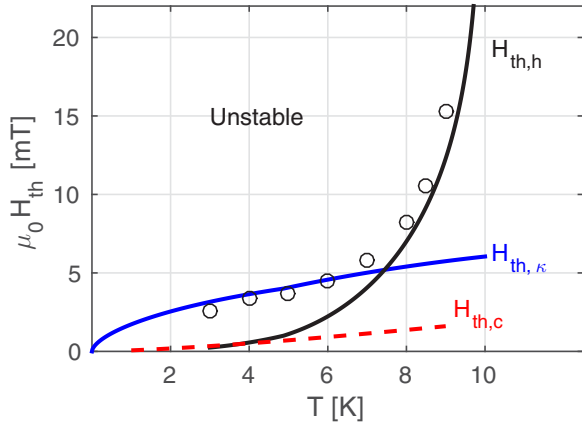
FIG. 3. Threshold magnetic fields $H_{th,\kappa}$ (blue), $H_{th,h}$ (black), and $H_{th,c}$ (dashed red) as functions of temperature. The discrete points represent the numerical results.

FIG. 4. Temporal variations in temperature prior to avalanches at 5, 7 and 9 K.

To verify the validity of the derived predictions near the instability onset, the set of full equations (3)–(5) were solved numerically using the procedure described in Ref. [30]. Material parameters typical for MgB$_2$ films [30,31] were used, i.e., $T_c = 39$ K, $c_0 = 35 \times 10^3$ J/m, $\kappa_0 = 160$ W/K m^3, $\rho_n = 7 \times 10^{-8}$ Ω m, $j_{c0} = 1 \times 10^{11}$ A m^{-2}, and $n_0 = 50$. The creep exponent was limited to $n = 400$ at low temperatures. The field ramp rate was set to $\mu_0 \dot{H}_a = 600$ mT/s, and the sample dimensions were $w = 2$ mm and $d = 0.5$ μm. The substrate cooling parameter, not known from measurements, was taken as $h_0 = 1.8 \times 10^4$ W/K m^2 to give a threshold temperature near 10 K, in accordance with experimental observations [21]. Numerical results were obtained for temperatures down to 3 K.

Figure 3 shows the threshold magnetic field as a function of temperature. The full curves represent the analytical expressions $H_{th,\kappa}$ and $H_{th,h}$, while the discrete data show the simulation results. Each data point indicates the applied field when the first dendritic avalanche occurred as the field increased from zero. At $T = 9.5$ K, the simulations stopped generating avalanches. From the figure one sees that for $T < 7$ K, the graph representing $H_{th,\kappa}$ fit the numerical data very well. From 7 K the data cross over to follow closely the curve representing $H_{th,h}$. The dashed curve represents the adiabatic threshold field, $H_{th,c}$, which clearly does not fit the simulation results at any temperature; see below for more discussion.

Direct evidence for oscillatory behavior preceding the onset of avalanches is presented in Fig. 4. The figure shows temporal fluctuations in the excess temperature, $\Delta T = \max\{\tilde{T}\} - T$, over an interval of 0.5 ms prior to avalanche events at $T = 5$, 7, and 9 K. The t_0 is the time of avalanche onset, defined as when $\max\{\tilde{T}\} = T_c$. The graph obtained at 9 K shows in the whole time interval clear oscillations with one dominant frequency. During the last 0.1 ms before $t = t_0$, the amplitude is growing significantly. A quite similar behavior is evident also in the graph obtained at $T = 7$ K. The oscillations here are smaller in amplitude, and noise is more pronounced. Nevertheless, nearly harmonic oscillations occur during the last 0.3 ms before onset, and their frequency is larger than at 9 K. As in the curve for 9 K, the oscillation amplitude increases toward the onset. In addition, the dc part of the ΔT signal also
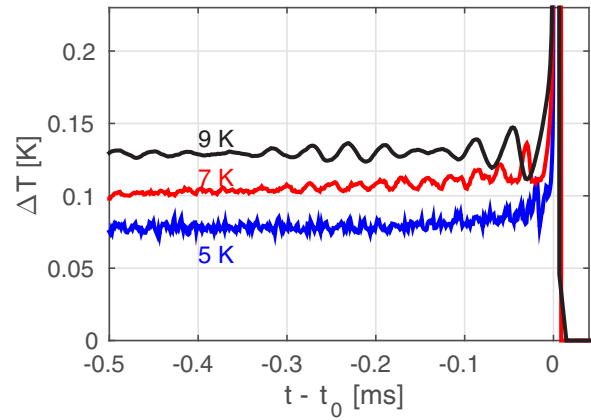
increases slightly toward time t_0. At 5 K, on the other hand, rapid fluctuations dominate the behavior, and a characteristic frequency is not present. The dc part of ΔT increases also here when approaching the time of onset.

The characteristic frequency, ω, found from the simulation results at temperatures between 6 and 9 K is plotted as discrete data in Fig. 5. The ω was obtained from the location of the peak in the Fourier spectrum of $\Delta T(t)$, prior to the first avalanche occurring at each temperature. The full curves in the figure represent the analytical expressions ω_κ and ω_h. One sees that the decrease in ω with increasing temperature is following the curves for $\omega_h(T)$ and $\omega_\kappa(T)$ very well.

Regarding the adiabatic condition, i.e., when the instability is prevented only by the heat capacity of the superconductor, the threshold field follows from Eq. (6) with $\kappa = h = 0$. Using k_x with $l(H_a)$ from Eq. (1) in the shallow penetration limit, one finds

$$H_{th,c} = \sqrt{\frac{2}{\pi}\frac{cT^*}{\mu_0}\frac{d}{w}}. \tag{14}$$

This expression was obtained previously [17,18]. It is also noteworthy here that this threshold is associated with oscillations, and the frequency is contained in Eq. (7). However, for the material parameters and field ramp rate used in our simulations, the frequency curve falls far outside the scale in Fig. 5, signaling that the adiabatic limit in this case is not
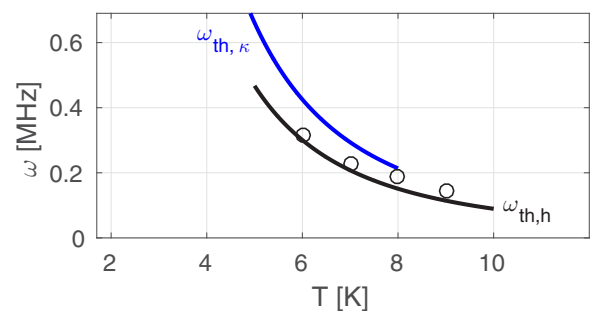
FIG. 5. Oscillation frequency as a function of temperature. The discrete data represent the numerical results, while the full curves are from theory.

relevant at any temperature. This is fully consistent also with the poor fit of the curve $H_{\mathrm{th},c}(T)$ to the numerical data in Fig. 3.

Finally, it is interesting to compare the onset thresholds obtained for the different oscillatory regimes with those from previous works, where only nonoscillatory modes were considered. In Ref. [19], the following expression was obtained for the threshold electric field:

$$E_{\mathrm{th}} = \frac{T^*}{j_c}\left(\frac{\pi}{2l}\sqrt{\kappa} + \sqrt{\frac{h}{nd}}\right)^2. \tag{15}$$

By direct comparison, it follows that this threshold is higher than the oscillatory thresholds derived in the present work. For example, in the case when $h = 0$, the E_{th} in Eq. (15) is a factor n larger than $E_{\mathrm{th},\kappa}$ of Eq. (8). Thus, in an increasing applied magnetic field, the onset condition for this oscillatory regime will be met long before that of the nonoscillatory instability.

In conclusion, several oscillatory regimes of the thermomagnetic instability in superconducting films were analyzed, and explicit onset conditions, i.e., threshold temperature and electric and applied magnetic field, were obtained as functions of material parameters and field ramping rate. The analytical work was supplemented by numerical simulations, and both confirm that oscillatory modes are more unstable than the conventional ones. The results show that large-scale avalanches can nucleate directly from the Bean critical state, rather than being mediated by nonthermal microavalanches, which up to now was the most plausible explanation for the occurrence of dendritic avalanches in films during slow field variations. The work provides predictions also of the characteristic oscillations frequency, and thus it calls for new experiments investigating the nucleation mechanisms for thermomagnetic avalanches in superconducting films.

[1] C. P. Bean, Rev. Mod. Phys. **36**, 31 (1964).

[2] S. L. Wipf, Phys. Rev. **161**, 404 (1967).

[3] P. S. Swartz and C. P. Bean, J. Appl. Phys. **39**, 4991 (1968).

[4] R. G. Mints and A. L. Rakhmanov, Rev. Mod. Phys. **53**, 551 (1981).

[5] S. L. Wipf, Cryogenics **31**, 936 (1991).

[6] A. L. Rakhmanov, D. V. Shantsev, Y. M. Galperin, and T. H. Johansen, Phys. Rev. B **70**, 224502 (2004).

[7] L. Legrand, I. Rosenman, C. Simon, and G. Collin, Physica C **211**, 239 (1993).

[8] R. G. Mints, Phys. Rev. B **53**, 12311 (1996).

[9] M. R. Wertheimer and J. le G. Gilchrist, J. Phys. Chem. Solids **28**, 2509 (1967).

[10] Ch. Jooss, J. Albrecht, H. Kuhn, S. Leonhardt, and H. Kronmüller, Rep. Prog. Phys. **65**, 651 (2002).

[11] P. Leiderer, J. Boneberg, P. Brüll, V. Bujok, and S. Herminghaus, Phys. Rev. Lett. **71**, 2646 (1993).

[12] V. Vlasko-Vlasov, U. Welp, V. Metlushko, and G. W. Crabtree, Physica C **341–348**, 1281 (2000).

[13] T. H. Johansen, M. Baziljevich, D. V. Shantsev, P. E. Goa, Y. M. Galperin, W. N. Kang, H. J. Kim, E. M. Choi, M.-S. Kim, and I. Lee, Europhys. Lett. **59**, 599 (2002).

[14] M. S. Welling, R. J. Westerwaal, W. Lohstroh, and R. J. Wijngaarden, Physica C **411**, 11 (2004).

[15] R. G. Mints and E. H. Brandt, Phys. Rev. B **54**, 12421 (1996).

[16] I. S. Aranson, A. Gurevich, M. S. Welling, R. J. Wijngaarden, V. K. Vlasko-Vlasov, V. M. Vinokur, and U. Welp, Phys. Rev. Lett. **94**, 037002 (2005).

[17] D. V. Shantsev, A. V. Bobyl, Y. M. Galperin, T. H. Johansen, and S. I. Lee, Phys. Rev. B **72**, 024541 (2005).

[18] D. V. Denisov, A. L. Rakhmanov, D. V. Shantsev, Y. M. Galperin, and T. H. Johansen, Phys. Rev. B **73**, 014512 (2006).

[19] D. V. Denisov, D. V. Shantsev, Y. M. Galperin, E.-M. Choi, H.-S. Lee, S.-I. Lee, A. V. Bobyl, P. E. Goa, A. A. F. Olsen, and T. H. Johansen, Phys. Rev. Lett. **97**, 077002 (2006).

[20] J. Albrecht, A. T. Matveev, J. Strempfer, H.-U. Habermeier, D. V. Shantsev, Y. M. Galperin, and T. H. Johansen, Phys. Rev. Lett. **98**, 117001 (2007).

[21] T. H. Johansen, M. Baziljevich, D. V. Shantsev, P. E. Goa, Y. M. Galperin, W. N. Kang, H. J. Kim, E. M. Choi, and S. I. Lee, Supercond. Sci. Technol. **14**, 726 (2001).

[22] E. H. Brandt, Phys. Rev. B **52**, 15442 (1995).

[23] M. Baziljevich, E. Baruch-El, T. H. Johansen, and Y. Yeshurun, Appl. Phys. Lett. **105**, 012602 (2014).

[24] S. Field, J. Witt, F. Nori, and X. Ling, Phys. Rev. Lett. **74**, 1206 (1995).

[25] C. J. Olson, C. Reichhardt, and F. Nori, Phys. Rev. B **56**, 6175 (1997).

[26] E. Altshuler and T. H. Johansen, Rev. Mod. Phys. **76**, 471 (2004).

[27] I. Guillamón, H. Suderow, S. Vieira, J. Sesé, R. Córdoba, J. M. De Teresa, and M. R. Ibarra, Phys. Rev. Lett. **106**, 077001 (2011).

[28] E. H. Brandt and M. Indenbom, Phys. Rev. B **48**, 12893 (1993).

[29] J. I. Vestgården, Y. M. Galperin, and T. H. Johansen, J. Low Temp. Phys. **173**, 303 (2013).

[30] J. I. Vestgården, D. V. Shantsev, Y. M. Galperin, and T. H. Johansen, Phys. Rev. B **84**, 054537 (2011).

[31] J. R. Thompson, K. D. Sorge, C. Cantoni, H. R. Kerchner, D. K. Christen, and M. Paranthaman, Supercond. Sci. Technol. **18**, 970 (2005).